Cell Communication and Signaling

RESEARCH

Open Access

Aberrant expression of GTPase-activating protein ARAP1 triggers circular dorsal ruffles associated with malignancy in hepatocellular carcinoma Hep3B cells

Xiaowei Sun[1†], Yanan Li[1†], Yuxin He[1], Longjiao Cheng[1], Li Wang[1], Jinzi Wei[1], Jianan Chen[2], Linxuan Du[1], Zhongyang Shen[2,3,4], Yan Xie[5,6*], Adam C. Midgley[1,7*], Wentao Jiang[5,6*] and Sei Yoshida[1,3,8,9*]

Abstract

Background Circular dorsal ruffles (CDRs) are large and rounded membrane ruffles that function as precursors of macropinocytosis. We recently reported that CDRs form in Hep3B hepatocellular carcinoma (HCC) cells, but not in Huh7 and HepG2 HCC cells or LO2 cells, suggesting that an unknown molecular mechanism implicates CDRs in Hep3B malignancy through macropinocytosis uptake of excessive extracellular nutrients. In this study, we investigated the cellular role and the mechanism of CDRs in Hep3B cells by focusing on the GTPase-activating protein ARAP1.

Methods ARAP1 knock-out (KO) cells were generated. Confocal microscopy and high-resolution scanning electron microscopy (SEM) were used for identification of the target proteins and structure analysis, respectively. Proteasome inhibitor MG132, mitochondrial function inhibitor CCCP, ARF1 inhibitor Golgicide A, and macropinocytosis inhibitor EIPA were used to investigate the molecular mechanism. Cell proliferation and Transwell migration/invasion assays were used to investigate the role of ARAP1 in cellular malignancy.

Results ARAP1 was localized to CDRs, which had reduced size following ARAP1 KO. CDRs comprised small vertical lamellipodia, the expression pattern of which was disrupted in ARAP1 KO cells. Extracellular solute uptake, rate of cell growth, and malignant potential were attenuated in KO cells. ARAP1 was also localized to mitochondria in Hep3B cells but not in the control cell lines. Mitochondrial fission protein was increased in KO cells. CCCP treatment blocked CDRs in Hep3B cells but not in controls. Surprisingly, ARAP1 expression level in Hep3B cells was lower than in Huh7, HepG2, and LO2 cells. MG132 treatment increased the ARAP1 levels in Hep3B cells, but not in Huh7 cells, revealing that ARAP1 is actively degraded in Hep3B cells.

[†]Xiaowei Sun and Yanan Li co-first authors.

*Correspondence:
Yan Xie
dr.xieyan@nankai.edu.cn
Adam C. Midgley
midgleyac@nankai.edu.cn
Wentao Jiang
jiangwentao@nankai.edu.cn
Sei Yoshida
seiyoshi@nankai.edu.cn
Full list of author information is available at the end of the article

Conclusions These results strongly suggest that the aberrant expression of ARAP1 in Hep3B cells modulates CDRs via mitochondrial function, thereby resulting in excess uptake of nutrients as an initial event in cancer development. Based on these findings, we propose that the molecular mechanisms underlying the formation of CDRs, focusing on ARAP1, may serve as an effective therapeutic target in some types of HCC and cancers.

Keywords Circular dorsal ruffles, Macropinocytosis, ARAP1, Hepatocellular carcinoma

Background

Circular dorsal ruffles (CDRs) are enlarged and rounded membrane ruffles that form on the dorsal surface of cells [16, 20, 59]. In response to stimulation with extracellular ligands, such as platelet-derived growth factor (PDGF), epidermal growth factor (EGF), hepatocyte growth factor (HGF), and insulin; cells induce the surface development of vertical membrane ruffles to produce these CDRs, in which the ruffles bend inward and gradually envelop the open area to generate vesicles [59]. It has accordingly been proposed that CDRs are involved in macropinocytosis, a large-scale type of endocytosis that facilitates the uptake of extracellular solutes [12, 16, 20]. Live-cell imaging of CDRs in mouse embryonic fibroblasts (MEFs) and human glioblastoma LN299 cells clearly show that large-sized vesicles (macropinosomes) are generated upon the closure of CDRs [59, 61]. Since CDRs were originally identified in PDGF-stimulated human glial cells in 1983 [34], the structures have been confirmed in more than 15 different cell types, including mouse embryonic fibroblasts (MEFs) [59], mouse fibroblast NIH-3T3 cells [14], mouse podocyte MPC5 cells [18], human glioblastoma LN229 cells [61], and hepatocellular carcinoma (HCC) Hep3B cells [46].

In terms of the molecular mechanism of CDR formation, numerous studies have focused on the roles of small GTPases [20]. For example, Rac1 has been detected in CDRs [17], and it was demonstrated that overexpression of the active form of Rab5a induces CDRs, whereas the effect was diminished by expression of the dominant-negative form of Rac [37]. Moreover, co-expression of the dominant-active form of Ras and wild-type Rab5a has been shown to induce CDRs in MEFs [29]. Similarly, the role of the ARF family of small GTPases and associated signaling molecules have been implicated in the process. To date, six different ARFs have been identified in mammalian cells, although humans lack ARF2 and thus, only five of these are expressed [49]. Among the ARFs, ARF1, 5, and 6 have been shown to be localized in CDRs [14, 53]. In common with other small GTPases, ARFs are negatively regulated by GTPase-activating proteins (GAPs). There are more than 15 ARF GAPs, and 6 of them (ACAP1, ACAP2, AGAP1, ASAP1, ASAP3, and ARAP1) have been shown to be involved in the formation of CDRs [50]. Overexpression studies have revealed that ACAP1, ACAP2, and AGAP1 inhibited the development of CDRs [21, 35]. Knockdown of ASAP1 was shown to result in an increased number of cells showing CDRs [8]. Furthermore, ASAP3 has been detected at CDRs [13] and ARAP1 has been established to regulate the size of CDRs via ARF1/5 [14].

Certain types of cancer cells are reported to be characterized by the development of CDRs, with growth factor stimulations being shown to induce CDRs in human pancreatic cancer PANC1 cells [36], mouse epithelial tumor Mgat5 cell line [5], and mouse melanoma 2054E cells [25]. Trastuzumab, a monoclonal antibody that targets human ERBB2 (HER2) was found to induce CDRs in the human breast cancer SK-BR-3 cell line [4]. In human glioblastoma LN229 cells, the growth arrest-specific 6 (GAS6) protein induces CDRs, which promotes macropinocytosis and contributes to the focal adhesion turnover in these cells [61]. Furthermore, we have recently found that growth factor (GF) treatment induced CDRs in the human Hep3B HCC cell line, although not in other HCC cell lines, such as HepG2 and Huh7, or in the LO2 cell line [46]. Given that macropinocytosis functions in the uptake of extracellular solutes, it has been proposed that heightened nutrient uptake via macropinocytosis in cancer cells triggers sufficient cell growth resulting in tumor development [39, 41, 48, 58]. On the basis of these findings, we hypothesized that the development of CDRs in certain cancer cells is associated with abnormally high levels of macropinocytosis, thereby contributing to the uptake of excess amounts of nutrients and thus promoting rampant tumor growth [46]. The differential molecular mechanisms that govern the formation of CDRs in Hep3B, but not in other HCC cell lines, remains unclear.

Interestingly, the ARF-GAP ARAP1 (Arf-GAP with Rho-GAP domain, Ankyrin repeat and PH domain 1), which is involved in CDR formation, has also been suggested to play a role in the development of cancer. ARAP1 antisense RNA1 (ARAP1-AS1) has been found to enhance the levels of ARAP1 mRNA [57], and increases in ARAP1-AS1 expression have been reported in human gastric cancer [22]. Moreover, a low level of ARAP1-AS1 expression has been demonstrated to be associated with an inhibition of lung cancer proliferation [51], and silencing ARAP1-AS1 has the effect of suppressing the proliferation of breast cancer cells [33]. Although several

studies have proposed the molecular mechanisms by which ARAP1-AS1 modulates tumor development such as in bladder cancer [52, 63], renal cell carcinoma [65]; and ovarian cancer [30], the roles of ARAP1 and ARAP1-AS1 (as the antisense RNA of ARAP1) in cancer development have yet to be sufficiently determined. It could be hypothesized that ARAP1 is involved in cancer development via CDR formation.

In this study we investigated the molecular mechanisms regulating the formation of CDRs in Hep3B cells, focusing on the function of ARAP1 in the context of cancer development. We found that ARAP1 was expressed at the CDRs of Hep3B cells, and observed reductions in the size of CDRs, extracellular solute uptake efficiency, and rate of cell growth in ARAP1 knock-out (KO) cells. Invasion and migration assays showed that ARAP1 KO attenuated malignancy. We also revealed that ARAP1 was uniquely expressed at the mitochondria in Hep3B cells, but not in control cells. Inhibition of mitochondrial function blocked the formation of CDRs in Hep3B cells, but not in MPC5 control cells. The mitochondrial distribution pattern was altered in ARAP1 KO cells and we found that the expression level of FIS1, a mitochondrial fission protein [3, 19], was increased in ARAP1 KO cells. These findings suggest an interaction between mitochondrial function and the formation of CDRs in Hep3B cells. Collectively, we provide evidence that aberrant ARAP1 expression in Hep3B cells induces the formation of CDRs via modulation of mitochondrial function, leading to increased nutrient uptake, which in turn triggers the development of cancer.

Methods

Reagents and antibodies

Recombinant human EGF (AF-100-15) and human HGF (100–39 H) were purchased from Peprotech (Cranbury, USA). Recombinant human insulin (M9194) was purchased from AbMole (Houston, USA). The ARF1 inhibitor Golgicide A (HY-100540) was obtained from MedChemExpress (Monmouth Junction, USA); EIPA (1154-25-2) was obtained from Tocris (Bristol, UK); CCCP (HY-100941) and Brefeldin A (Hy-16592) were obtained from MedChemEepress (Monmouth Junction, NJ, USA); MG132 (GC10383) was obtained from GLPBIO (California, USA); protease inhibitor cocktail (04,693,159,001) was purchased from Roche (Basel, Switzerland); and rhodamine phalloidin (RM02835) was purchased from ABclonal (Wuhan, China). Anti-AKT (#9272) and pAKT (Ser473) (#4060) antibodies, used for western blot analysis, were purchased from Cell Signaling Technology (Danvers, USA); anti-ARAP1 (A10466), anti-β-Actin (AC004), and anti-GFP (AE012) antibodies, used for western blot analysis, were purchased from ABclonal; anti-FIS1 antibody (TA369131), used for western blot analysis, was purchased from ORIGENE (Rockville, MD, USA); anti-NUMB (A9352), used for immunofluorescence staining, was obtained from ABclonal; anti-ARF1 (10790-1-AP), anti-ARF6 (20225-1-AP), anti-TOM20 (11802-1-AP), and anti-Golgin97 (12640-1-AP) antibodies, used for immunofluorescence staining, were obtained from Proteintech (Wuhan, China); anti-TIM23 (611222). used for immunofluorescence staining, was obtained from BD Biosciences (San Jose, USA); and anti-ARAP1 (HPA012412), used for immunohistochemistry staining, was obtained from Sigma (St. Louis, MO, USA).

Cell culture and inhibitor treatment

Hep3B, HepG2, and MPC5 cells were purchased from Tongpai Biotechnology (Shanghai, China). Huh7, LO2, 293T, and NIH-3T3 cells were purchased from Hunan Fenghui Biotechnology (Changsha, Hunan, China). Cells were cultured in Dulbecco's modified Eagle's medium (DMEM: C12430500BT; Gibco) supplemented with 10% fetal bovine serum (FBS: FS301-02; TransGen Biotech, Beijing, China), penicillin (B25911; Shanghai Yuanye Bio-Technology), and streptomycin (A610494-0050; Sangon Biotech, Shanghai, China). To prevent mycoplasma contamination, cells were treated with prophylactic plasmocin (ant-mpp; InvivoGen, San Diego, USA), according to the manufacturer's instructions. For inhibitor treatments, cells were pre-treated with Golgicide A (10 μM) for 60 min or with CCCP (10 μM) for 6 h. For MG132 treatment, cells were incubated with the drug (10 μM) for the indicated time points.

CDR assay

The CDR assay was performed as previously described [46]. To induce CDRs, cells were stimulated with EGF (1 μg/mL, 3 min), insulin (0.6 μg/mL, 3 min), and HGF (10 ng/mL, 5 min). More than 1000 cells from three independent experiments were observed to calculate the average number of CDRs per cell. Actin images were used to identify the structures.

Establishment of a stable ARAP1-deficient Hep3B cell line

CRISPR-based knockout cell lines were generated using the lentiCRISPRv2 vector obtained from Addgene, which expresses a single guide RNA, Cas9 protein, and puromycin resistance gene. The ARAP1 single guide RNAs were designed, synthesized, and cloned into the lentiCRISPRv2 vector. Two different single guide RNAs targeting the human ARAP1 were designed [sgARAP1-1$^{\#}$: 5′-CACCGAATAGCTGCGCCACACCCCA-3′ (forward) and 5′-AAAC TGGGGTGTGGCGCAGCTA TTC-3′ (reverse); sgARAP1-2$^{\#}$: 5′-CACCGAGCC AGAGTGATGACCAAGA-3′ (forward) and 5′-AAAC

TCTTGGTCATCACTCTGGCTC-3′ (reverse); and sgARAP1-3#: 5′-CACCGCCACCCGTGCCGCCCC GCAC-3′ (forward) and 5′-AAACGTGCGGGGCGG CACGGGTGGC-3′ (reverse)]. An empty lentiCRISPRv2 plasmid was used as the control vector. 293T packaging cells from Hunan Fenghui Biotechnology (Changsha, Hunan, China) were seeded in 10-cm culture dishes and subsequently co-transfected with 4 μg sgRNA plasmid or empty lentiCRISPRv2 plasmid, 1 μg pVSVg (AddGene 8454) and 3 μg psPAX2 (AddGene 12260) using Lipofectamine 2000 (Invitrogen, Carlsbad, CA, USA). Following 24- or 48-h incubations, 293T cell supernatants were harvested by centrifuging for 10 min at 1000 rpm, then filtered through 0.45-μm membrane filters. The supernatants containing the virus were used to infect Hep3b cells for 6 h. After selection with puromycin (5 μg/mL) for 3 days, the knockout efficiency was assessed by western blot analysis and the confirmed KO cells were used in subsequent experiments.

Construction of GFP-ARAP1 plasmid (pGFP-ARAP1) and the transfection

The plasmid pGFP-ARAP1 was generated by GentleGen Science and Technology Ltd (Suzhou, Jiangsu, China). ARAP1 sequences were constructed based on the human transcript variant 3 mRNA (NCBI Reference: NM 001040118.3) and subcloned into the pEGFP-N1 vector (BR083; Fenghui Biology, Changsha, China) using the BamH1 and Age1 sites. The ARAP1 sequence that was cloned into the resulting plasmid was confirmed by another company (Beijing Tsingke, Beijing, China). Plasmids were purified using the TIANpure Midi Plasmid Kit (DP107-02; TIANGEN, Beijing, China). GeneTwin (TG101-02; Biomed, Beijing, China) was used for transfection according to the manufacturer's protocol.

Immunofluorescence staining and confocal microscopy

Cells were cultured overnight on coverslips in low-glucose DMEM without FBS. After stimulation with growth factors, the cells were fixed in fixation buffer A (4% paraformaldehyde (PFA) in phosphate-buffered saline (PBS), pH 7.4) for 20 min at room temperature (RT) and washed in TBST (20 mM Tris, 150 mM NaCl, 0.1% Tween 20, pH 7.6). For immunofluorescence (IF) staining, cells were permeabilized in 0.1% Triton X-100 in PBS for 5 min and then incubated in blocking buffer (5% bovine serum albumin (BSA) in TBST) for 30 min at RT. For primary antibody treatment, all primary antibodies were diluted 1:50 in blocking buffer and incubated with samples overnight at 4 °C. Thereafter, the samples were washed with TBST (three times for 10 min at RT). As a secondary antibody treatment, samples were incubated for 2 h at RT with anti-rabbit IgG Alexa Fluor 488 (150081; Abcam, Boston, USA) and anti-mouse IgG Alexa Fluor 546 (Invitrogen A1003) diluted to 1:500 in the blocking buffer. The cells were then incubated for 1 h at RT with rhodamine phalloidin diluted 1:100 in TBST containing 5% BSA. The samples were subsequently washed three times with TBST for 10 min at RT and then mounted using mounting medium containing DAPI. Microscopic observations were performed using a Leica TCS SP5 confocal microscope at the Core Facility of the College of Life Sciences, Nankai University, China. To display the merged images, Alexa Fluor 546 images (shown as bright orange) and rhodamine-phalloidin images (shown as red-orange) were converted to the pseudocolor magenta using ImageJ software (version 2.14.0/1.54 f; National Institutes of Health).

Quantification of IF images

ImageJ software was used for image analysis. To quantify the size of the mitochondrial distribution area, the original images were converted into 8-bit images. Actin images were used to determine the area of the cells using the "polygon selection" tool. TOM20 or TIM23 images were used to generate the threshold images, from which we determined the area of mitochondria. The ratio of "area of the mitochondria"/"area of the cell" was calculated as the result. To quantify the ARAP1 signal at the mitochondria, TIM23 images were used to determine mitochondrial locations. A binary image map was produced from the TIM23 image. ARAP1 images and the binary images were combined using the "and" tool to generate images showing ARAP1 at mitochondria (ARAP1 at Mito). The ARAP1 signal areas in "ARAP1" and "ARAP1 at Mito" images were measured, then the ratio of "ARAP1 at Mito"/"ARAP1" was calculated. All experiments performed in this study were conducted in at least two biological replicates. The data are expressed as the means ± standard error of the mean.

Cell lysate preparation and western blotting

Cell lysates were prepared as previously described [46]. Briefly, the cells were lysed in cold lysis buffer (40 mM HEPES pH 7.5, 120 mM NaCl, 1 mM EDTA, 10 mM pyrophosphate, 10 mM glycerophosphate, 1.5 mM Na_3VO_4, 0.3% CHAPS, and a mixture of protease inhibitors) for 10 min. The lysates thus obtained were centrifuged at 13,000 × *g* for 15 min at 4 °C. and the resulting supernatants were mixed with 5× sodium dodecyl sulfate-polyacrylamide gel electrophoresis (SDS-PAGE) sample buffer (#E153; GenStar, Beijing, China) and boiled for 5 min. The samples were subjected to SDS-PAGE and subsequent western blotting using the indicated antibodies.

Scanning electron microscopy

Hep3B cells were cultured on coverslips with collagen (Type I solution from rat tail, Sigma C3867) and fixed in fixation buffer B (2.5% glutaraldehyde, 0.18 M Na_2HPO_4, 0.019 M KH_2PO_4, pH 7.2) after human EGF stimulation as previously described [46]. The samples were submitted to Yimingfuxing Bio (Beijing, China) for embedding, according to standard procedures. Observations were performed using a field emission scanning electron microscope (SEM; Apreo S LoVac, Thermo Fisher) at the Central Laboratory of Nankai University. To determine the angles between the small ruffles, supporting lines were drawn according to each ruffle. Image J was used to measure the angle at which the lines interested as the angle between the ruffles. The total number of small ruffles of Control ($n=25$), KO1 ($n=25$), and KO2 ($n=18$) were observed from at least five different SEM images. Averages and standard deviations were calculated, and the one-way ANOVA statistical test was used to determine statistical significance.

FDx70 assay

Cells were cultured overnight on coverslips in low-glucose DMEM without FBS. Following the additions of EGF (1 μg/mL) or HGF (10 ng/mL) and fluorescein isothiocyanate-labeled dextran with an average molecular weight of 70,000 (FDx70, 0.5 mg/mL) (D1822; Invitrogen), the cells were incubated at 37 °C for 5, 10, 15, 30, and 60 min. Thereafter, the cells were fixed with 4% paraformaldehyde in PBS at RT for 20 min, washed three times with DPBS (B220KJ; BasalMedia, Shanghai, China) for 10 min, and mounted. For each sample, we obtained at least 10 phase-contrast and FITC-FDx70 images using a Live Cell Station (Zeiss Axio Observer Z1) at the Core Facility of the College of Life Sciences of Nankai University. Cell numbers were determined from phase contrast images and the number of induced macropinosomes was determined by counting FDx70-positive vesicles. The ImageJ software was used to measure the intensity of FDx70.

Cell counting Kit-8 cell proliferation assay

Cell Counting Kit-8 (CCK-8) cell proliferation assays were carried out as described previously [31]. Briefly, cells were seeded in the wells of 96-well plates (TCP010096; BioFil, Guangzhou, China) at a density of approximately 2000 cells per well (100 μL/well), with each treatment being assessed in five replicate wells. Thereafter, cell proliferation was examined daily up to 5 days, after which. 10 μL of CCK-8 solution (CK04; Dojindo Laboratories, Kumamoto, Japan) was added to the wells followed by incubation for 2 h at 37℃. The absorbance of wells was subsequently measured at 450 nm using a Multiskan FC microplate reader (Thermo Fisher Scientific).

Transwell migration and invasion assays

To assess cell migration and invasion, we used 24-well plates containing Transwell chambers of 8 μm size (TSC020024; BioFil). As the chemoattractant, 10% FBS was used [38]. For the migration assays, cells were harvested and resuspended in DMEM without FBS at a concentration of 5×10^5/mL. A 100-μL aliquot of the cell suspension was seeded in the upper chambers, and 500 μL of DMEM supplemented with 10% FBS was placed in the lower chambers. Cells were incubated for 48 h, after which the medium was removed from the Transwell chambers, non-migrating cells were removed from the upper chambers using a cotton swab. The upper chambers were then washed three times with PBS, and cells were fixed with 4% paraformaldehyde in PBS. Thereafter. the cells were stained for 20 min at RT with 600 μL of 1% crystal violet (C805211; MACKLIN, Shanghai, China). The upper chambers were washed a further three times with PBS (each for 10 min), and the number of the cells in the upper chambers was counted using a LeicaDFC420C light microscope. For the invasion assays, the Transwell chambers were pre-treated with Matrigel (354234; Corning) diluted 1:50 with DMEM for 1 h at 37℃, after which, 1 mL of cells was placed in the upper chamber at a concentration of 2×10^5/mL. The remaining procedures were carried out as described for the migration assay.

Statistical analysis

GraphPad Prism software (version 8.0; GraphPad Software) was used for statistical analyses. We performed a one-way ANOVA (for Figs. 1E, 2B, 5B and C, 8H and I and 9B and D; Supplementary Fig. 2B and D; Supplementary Fig. 3E; Supplementary Fig. 6B and C), two-tailed unpaired Student's *t*-test (for Fig. 7C and E), two-tailed paired Student's *t*-test (for Figs. 4A, 6I and J and 8C-F; Supplementary Fig. 6D; Supplementary Fig. 8D), one-tailed unpaired Student's *t*-test (for Fig. 6D), and frequency distribution (for Supplementary Fig. 1D and Supplementary Fig. 3A). For all analyses, a *p*-value of less that 0.05 was considered to signify a statistical significance.

Results

The GTPase-activating protein ARAP1, although not the target molecule ARF1, is located in the CDRs of Hep3B cells, and depletion of ARAP1 alters CDR size

To characterize the role of CDRs in the activity of Hep3B cells, we generated knockout (KO) cells in which the molecular mechanisms underlying CDR formation were attenuated. In this regard, we decided to generate ARAP1 KO cells, as it has previously been demonstrated that ARAP1 regulates the size of CDRs in NIH-3T3 cells [14]. Initially, we sought to determine whether, as

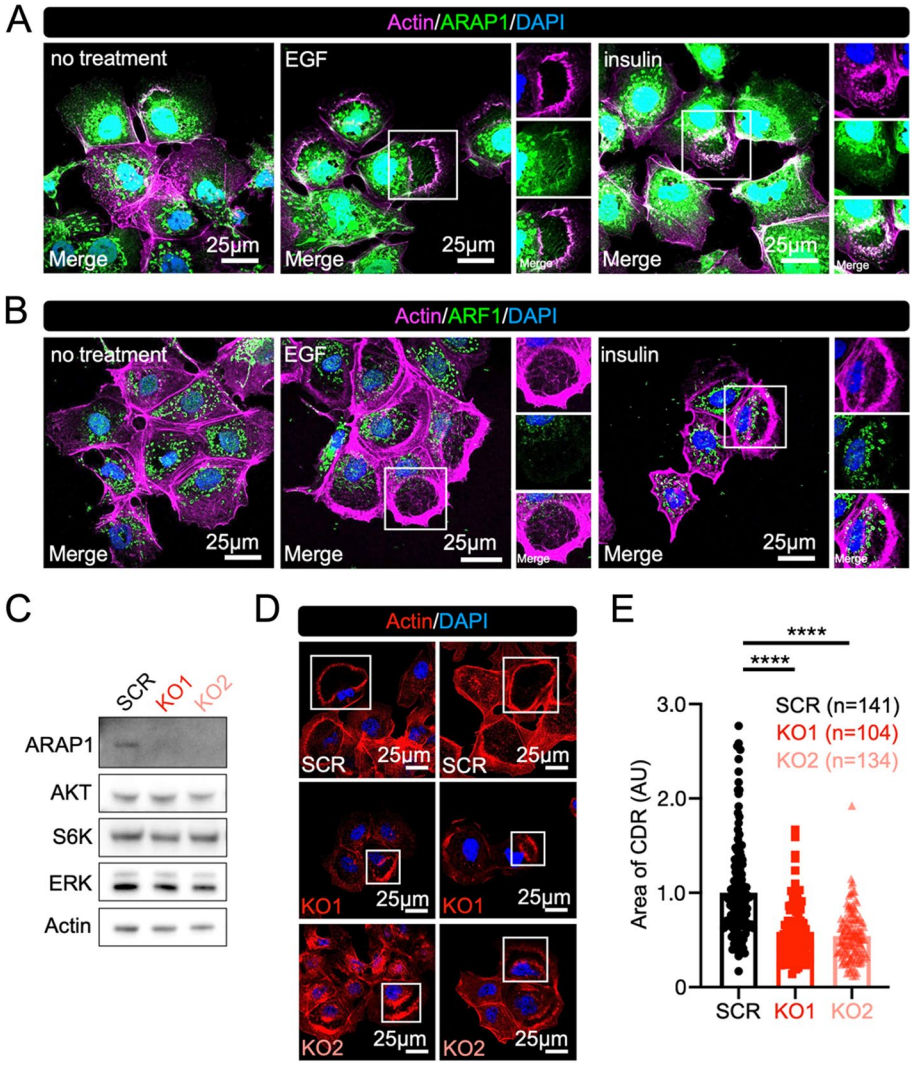

Fig. 1 ARAP1 modulates the size of CDRs in cells of the Hep3B hepatocellular carcinoma cell line. **A** and **B** Representative confocal images of Actin/ARAP1 (**A**) and Actin/ARF1 (**B**) with/without epidermal growth factor (EGF) and insulin. Actin was used to identify CDRs. **C** Western blot analysis was performed to confirm ARAP1 knock out (KO). AKT, S6K, ERK, and Actin are shown as the control. **D** Representative confocal images of CDR assays showing that the sizes of CDRs in the ARAP1 KO cells (KO1 and KO2) are smaller than those in the control cells (SCR: scramble). Two representative images are shown for each sample. **E** Quantification analysis of the size of CDRs induced by EGF treatment in the control (SCR, $n = 141$), KO1 ($n = 104$), and KO2 ($n = 134$) cells from two independent experiments. The average size of CDRs in the control cells was used as the standard. ****$p < 0.0001$ (one-way ANOVA). AU: arbitrary unit

in NIH-3T3 cells; ARAP1 and the target protein ARF1 are located at the growth factor (GF)-induced CDRs of Hep3B cells. Based on confocal microscopy observations, we accordingly established that ARAP1, although not ARF1, is expressed at the CDRs induced by EGF and insulin (Fig. 1A and B). It has previously been shown that the small GTPase ARF6 and the upstream signaling molecule NUMB1 are expressed in CDRs [67], and in the present study, we also observed that these molecules are recruited to the CDRs in Hep3B cells (Supplementary Fig. 1A and B). Having initially determined these distributions, we established two different ARAP1 KO cell lines, namely, KO1 and KO2. Western blot analysis (Fig. 1C) and immunofluorescence (IF) staining (Supplementary Fig. 1C) confirmed that the expression of ARAP1 was successfully depleted in both cell lines. Using these KO cell lines and the control cells, we performed a CDR assay, which revealed that the size of CDRs was reduced in the KO cells (Fig. 1D and E). We also compared the relative sizes of individual CDRs between control and KO cells. If the sizes of the CDRs were at least two-fold larger than average size of CDRs in the control

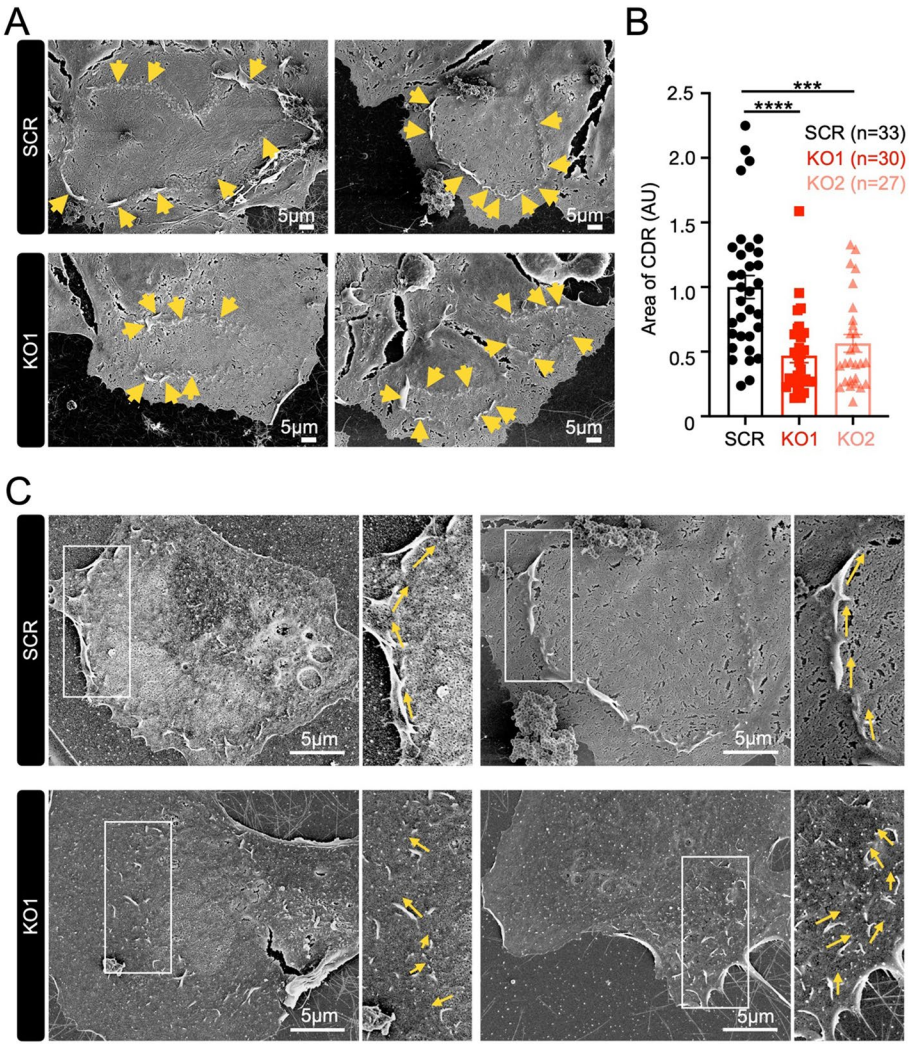

Fig. 2 High-resolution SEM observations revealed that the sizes of CDRs in KO cells were reduced and the expression patterns of vertical lamellipodia were disrupted. **A** Representative high-resolution SEM images of EGF-stimulated Hep3B cells showing CDRs consisting of small vertical ruffles (arrows) in both control (SCR) and KO (KO1) cells. Two representative images are shown for each sample. **B** Quantification of the sizes of CDRs in the control (SCR, $n = 33$), KO1 ($n = 30$), and KO2 ($n = 27$) cells. ****$p < 0.0001$; ***$p < 0.001$ (one-way ANOVA). AU: arbitrary unit. **C** Enlarged high-resolution SEM images showing details of the vertical ruffles (arrows). In contrast to the regular pattern of ruffles comprising the CDRs of the control (SCR) cells, the orientation of ruffles in the CDRs of KO (KO1) cells was disrupted. Two representative images are shown for each sample. Additional SEM images are shown in Supplementary Fig. 3

cells, we defined these CDRs as "large-sized" CDRs. We then found that "large-sized" CDRs were only observable in the control cells but not in the KO cells (Supplementary Fig. 1D). These findings indicated that ARAP1 is associated with a molecular mechanism that contributes to determining the size CDRs, particularly the formation of large-sized CDRs.

In a previous study, we showed that CDRs regulate GF-induced AKT phosphorylation (pAKT) in Hep3B cells [46], and in the present study, immunoblots revealed that the levels of pAKT in the KO cells were lower than those detected in the control cells, albeit not significantly (Supplementary Fig. 2A and B). Furthermore, IF staining of pAKT and AKT revealed that whereas the ratio of pAKT/AKT in the CDRs of KO1 cells was less than that for control cells, this difference was not detected in the KO2 cells (Supplementary Fig. 2C and D). Based on these observations, we concluded that although the depletion of ARAP1 contributes to a reduction in the size of CDRs, the difference is not sufficient to influence CDR-dependent pAKT.

Scanning electron microscopy observations revealed that CDRs comprise small-sized vertical lamellipodia, the expression pattern of which is disrupted in ARAP1 KO cells

To visualize the effects of ARAP1 depletion in the CDR formation, we performed high-resolution SEM. As we have reported previously [46], the SEM images obtained in the present study showed that small-size vertical lamellipodia form the circle-like structures defined as CDRs (Fig. 2A). Given that our confocal observations revealed that the overall average size was reduced (Fig. 1E) and that "large-sized" CDRs were not induced in the KO cells (Supplementary Fig. 1D), we also measured the area of CDRs using these SEM images. In line with expectation, we found that the average size of the CDRs in both KO1 and KO2 cells was significantly smaller that of CDRs in the control cells (Fig. 2B). Moreover, our examination of 33 micrographs revealed the presence of three "large-sized" CDRs in the control cells, whereas none of these structures were identified in the KO cells (Supplementary Fig. 3A). Interestingly, examination of high-magnification images revealed that whereas in the control cells, the small lamellipodia were regularly induced and collective formed the circle-like structures that are characteristic of CDRs, the orientation of these ruffles was disrupted in both KO1 (Fig. 2C) and KO2 (Supplementary Fig. 3B) cells. Indeed, quantification analysis indicated that the average angle size between each of the ruffles in the control cells was approximately 40 degrees, while those in KO1 and KO2 cells were approximately 80 degrees (Supplementary Fig. 3C-E). Moreover, the difference between the average degree size of control and KO cells was significant, whereas there was no significant difference between the average angle size in KO1 and KO2 cells (Supplementary Fig. 3E). Consequently, SEM observations provided evidence that ARAP1 determines the size of CDRs by modulating the distribution of individual small ruffles.

ARAP1 is specifically localized to the mitochondria in Hep3B cells

Confocal microscopy observations of ARAP1 and ARF1 signals revealed that the expression patterns of these molecules were specific, and presumably mitochondrially localized (Fig. 1A and B). Thus, we prepared different types of control cells to test whether the cellular localization of ARAP1 in other cells was also unique. The ARAP1 antibody used in this study is the only product verified for IF staining. Therefore, to validate ARAP1 imaging experiments, we verified the specificity of the antibody used for IF staining by generating a GFP-ARAP1 expression plasmid (Supplementary Fig. 4). GFP-ARAP1 or GFP was expressed in 293T cells. Western blot analysis showed that GFP-ARAP1 was detected by the anti-GFP antibody, as well as the anti-ARAP1 antibody we used (Supplementary Fig. 4A). Moreover, confocal microscopy confirmed that the ARAP1 antibody detected GFP-ARAP1, but not GFP, in the cells (Supplementary Fig. 4D). In a previous study, we reported that the HCC cell lines Huh7 and HepG2 cells did not express CDRs, and used these cell lines as controls for experiments using Hep3B cells [46]. Using Huh7 cells, we confirmed that this ARAP1 antibody detected GFP-ARAP1 expression in the cells by western blot analysis and confocal microscopy (Supplementary Fig. 4B and E). These results indicate that the ARAP1 antibody was specific and could be used for subsequent IF staining experiments.

To determine whether ARAP1 localized at the mitochondria, we used two well-established mitochondrial markers, TIM23 and TOM20 [43, 64]. TIM23/ARAP1 double staining clearly showed that ARAP1 was specifically co-localized with TIM23 in Hep3B cells (Fig. 3A and B). As control cell lines, we used Huh7 (Fig. 3C and D), HepG2 (Fig. 3E), and the LO2 cell line (Fig. 3F). Weak and partial co-localization of TIM23 and ARAP1 was observed in these cells. It has been shown that NIH-3T3 and podocyte MPC5 cells also presented CDRs [14, 18]. However, we did not observe ARAP1 localization at the mitochondria of these cells (Fig. 3G and H). In addition, colocalization of ARAP1 and TIM23 was not observed in 293T cells (Fig. 3I). These results indicated that the distribution pattern of ARAP1 in Hep3B cells was unique compared to that in the control cell lines.

ARAP1 expression in Hep3B cells is lower than in control cells

Interestingly, western blot analysis showed that the expression level of ARAP1 in Hep3B cells was lower than that in Huh7, HepG2, and LO2 cells (Fig. 4A). Notably, we were unable to express GFP-ARAP1 in Hep3B cells for unknown reasons (Supplementary Fig. 4C). These results suggest that ARAP1 expression in Hep3B cells is aberrant, presumably because the expression mechanism is disturbed or protein degradation mechanisms targeting the protein are activated. To test this line of thought, we incubated Hep3B cells with proteasome inhibitor MG132 for the indicated time points, and found that the expression level of ARAP1 increased approximately 2-fold after 2 h of MG132 treatment (Fig. 4B). As a control, the experiment was replicated using Huh7 cells, and the results showed that the treatment did not affect ARAP1 expression (Fig. 4C).

We also compared expression level and the distribution pattern of ARAP1 in Huh7 and Hep3B cells by confocal microscopy under the exact same experimental conditions. We observed that ARAP1 expression level

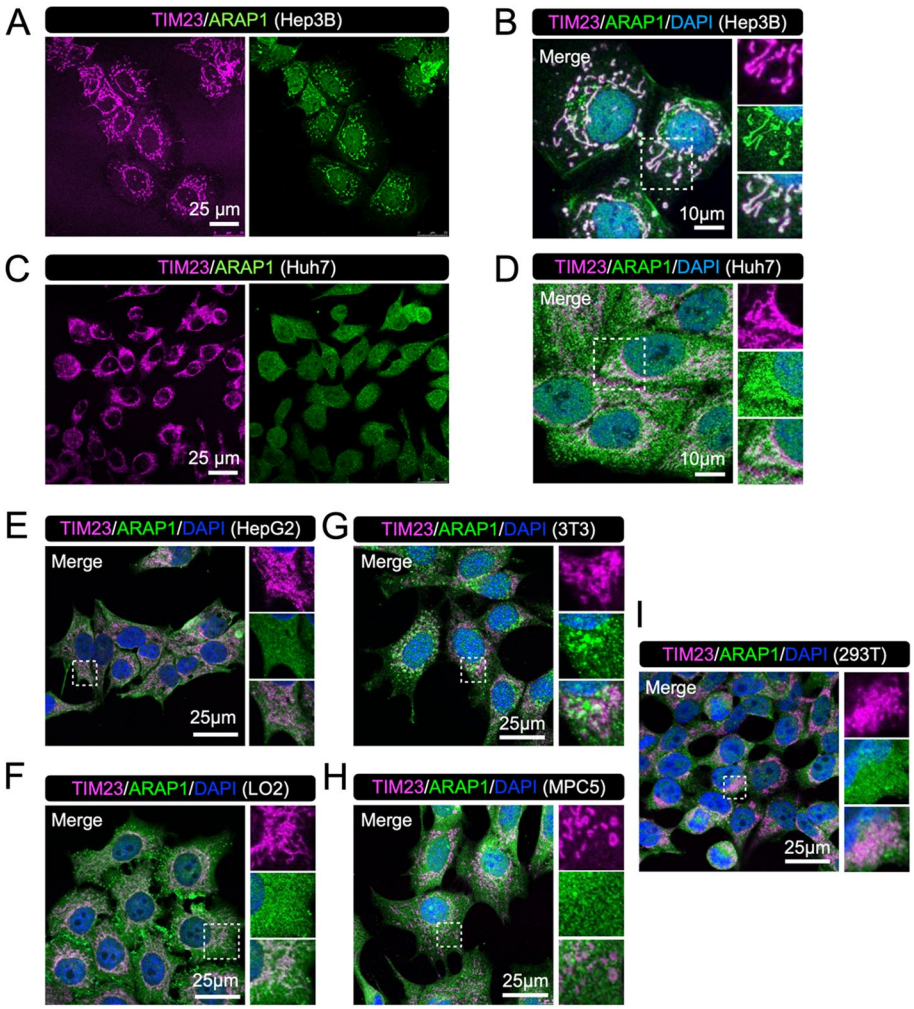

Fig. 3 ARAP1 is specifically localized to the mitochondria in Hep3B cells. **A**-**B** Representative confocal images of TIM23/ARAP1 in Hep3B cells without growth factor stimulation. Strong co-localization of TIM23 and ARAP1 was observed. Images are shown at low magnification (**A**) and high magnification (**B**). **C-D** Representative confocal images of TIM23/ARAP1 in Huh7 cells without growth factor stimulation. Weak co-localization of TIM23 and ARAP1 was observed. Images are shown at low magnification (**C**) and high magnification (**D**). **E-F** Representative confocal images of TIM23/ARAP1 in HepG2 (**E**) and LO2 (**F**) cells without growth factor stimulation. Weak co-localization of TIM23 (magenta) and ARAP1 (green) was observed. **G-H** Representative confocal images of TIM23/ARAP1 in NIH-3T3 (**G**) and MPC5 (**H**) cells without growth factor stimulation. Co-localization of TIM23 (magenta) and ARAP1 (green) was not observed. **I** Representative confocal images of TIM23/ARAP1 in 293T cells without growth factor stimulation. Co-localization of TIM23 (magenta) and ARAP1 (green) was not observed

was higher in Huh7 cells than in Hep3B cells and that ARAP1 expression was elevated in the nuclei of Huh7 cells (Supplementary-Fig. 5A). Interestingly, when we observed the distribution pattern of ARAP1 in Hep3B cells with/without MG132 treatment, we found that the expression level of ARAP1 in the nuclei was increased after treatment (Supplementary-Fig. 5B), suggesting an interaction between the ARAP1 degradation mechanism and its nuclear expression. Based on these results, we concluded that ARAP1 expression was aberrant in Hep3B cells compared to Huh7, HepG2, and LO2 cells.

The distribution pattern of mitochondria is changed in ARAP1 KO cells

Confocal microscopy observation of TIM23 suggested that Hep3B cells has a distinct distribution pattern of mitochondria, compared to the control cells (Fig. 3). To determine whether the mitochondrial localization of ARAP1 has any influence on the mitochondrial distribution pattern in Hep3B cells, we compared the cellular localization of TOM20 in controls and KO cells. Actin was used to identify the cell area, and the ratio of TOM20 to Actin was calculated as the "area of TOM20"/"cell

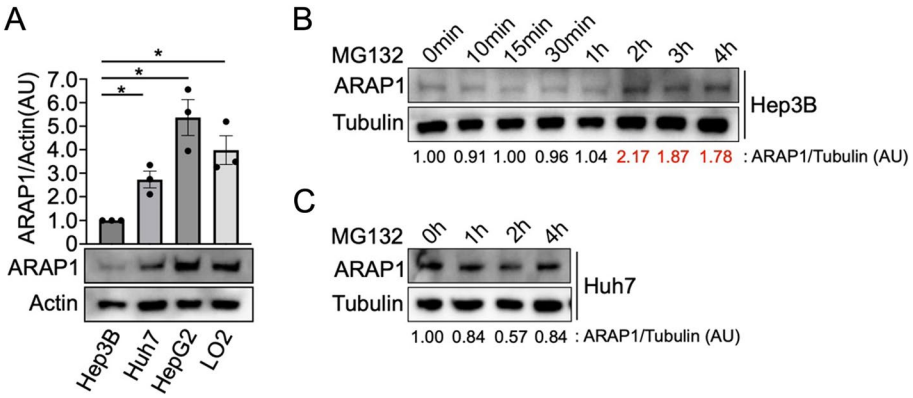

Fig. 4 ARAP1 is actively degraded in Hep3B cells. **A** Western blot analysis showed that ARAP1 expression level in Hep3B was lower compared to the control cells. Three independent experiments were carried out for the quantification. *$p < 0.05$ (two-tailed paired Student *t*-test). AU: arbitrary unit. **B**-**C** ARAP1 expression level was increased in Hep3B cells (**B**), but not in Huh7 cells (**C**), after 2 h of MG132 treatment (10μM). The numbers below each image are the ratio of the expression level of ARAP1 to that of tubulin. Representative western images are shown. AU: arbitrary unit

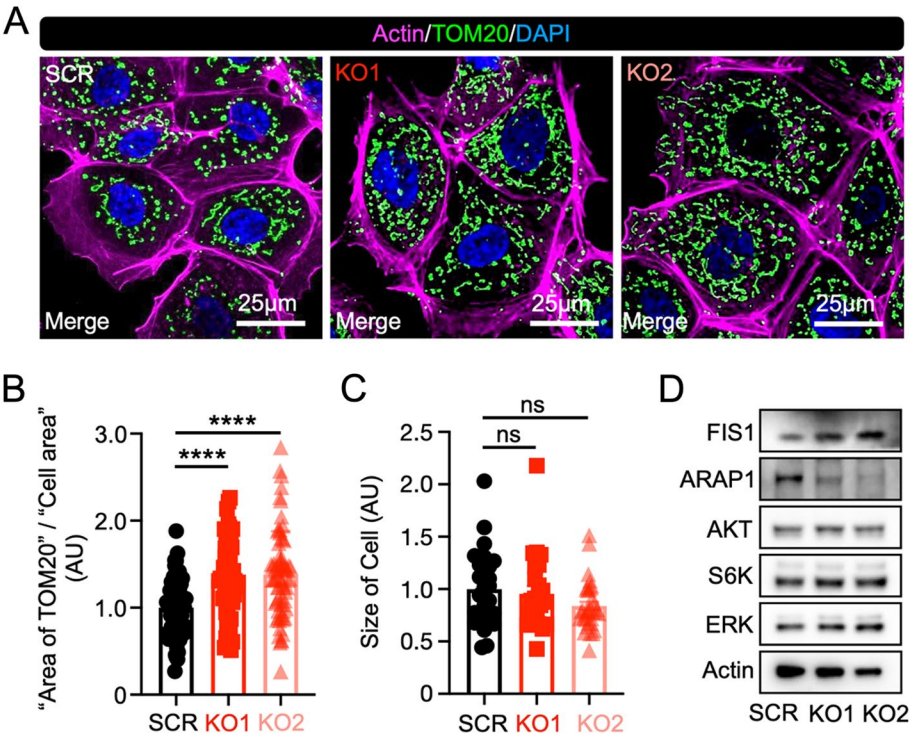

Fig. 5 Mitochondrial distribution patterns are disrupted in ARAP1 KO cells. **A** Representative confocal images of Actin/TOM20 staining in control (SCR) and knockout (KO1 and KO2) cells. The area of the TOM20 distribution pattern (green) was expanded in KO cells. **B** Quantitative analysis of the area of the TOM20 distribution pattern in different cell types. The area of the TOM20 distribution pattern and sizes of cells were measured using ImageJ software and the ratio of "area of TOM20"/"cell area." was calculated. The results revealed that the ratios obtained for KO cells were higher than those obtained for the control cells, thereby indicating that the mitochondrial distribution area increased in response to the deletion of ARAP1. $n = 64$ (SCR), 56 (KO1), and 71 (KO2), from two independent experiments. ****$p < 0.0001$ (one-way ANOVA). AU: arbitrary unit. **C** Quantitative analysis showing that cell sizes were not altered in response to deletion of ARAP1 as control data for (**B**). **D** Representative western blot analysis results showing that FIS1 expression was increased in ARAP1 KO cells (KO1 and KO2) compared to the control (SCR). AKT, S6K, ERK, and Actin are shown as the control. The results of western blot analysis using KO3 are shown in Supplemental Fig. 6D

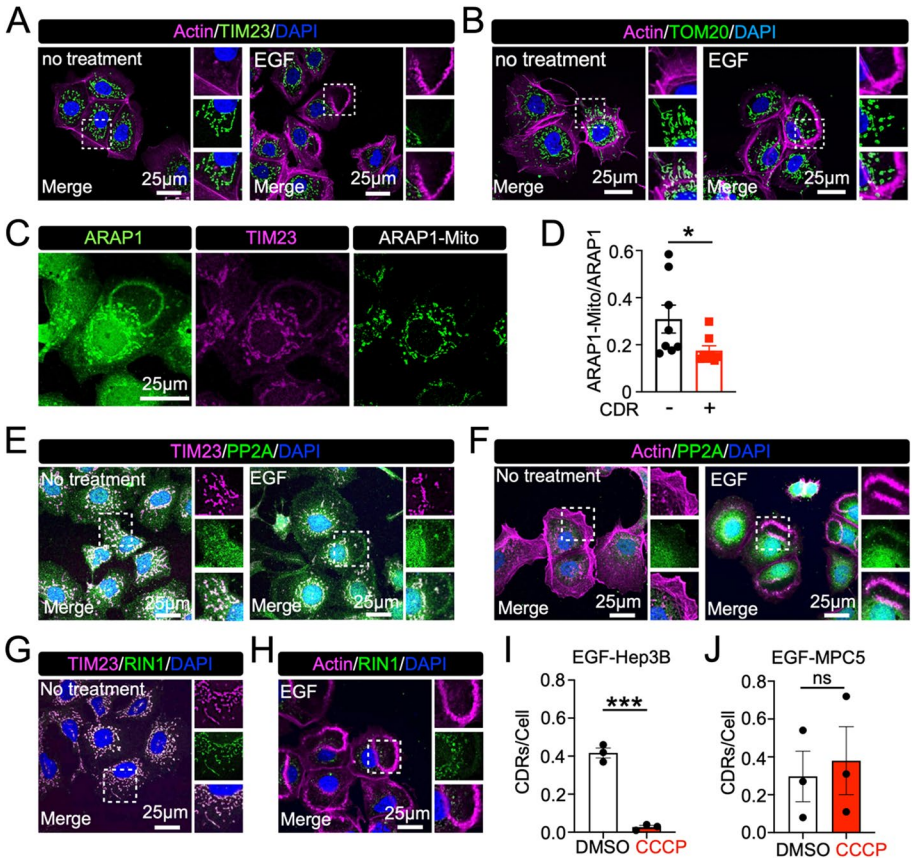

Fig. 6 There is an interaction between mitochondrial functions and CDR formation in Hep3B cells. **A** Representative confocal images of Actin/TIM23 in Hep3B cells with/without EGF stimulation. TIM23 was not detected in the circular dorsal ruffles (CDRs).**B** Representative confocal images of Actin/TOM20 in Hep3B cells with/without EGF stimulation. TOM20 was not detected in the CDRs. **C-D** The ARAP1 signal in mitochondria was reduced in cells with CDRs. Representative images used for the quantification are shown (**C**). Pseudo images showing ARAP1 at mitochondria (ARAP1-Mito) were generated based on ARAP1 and TIM23 images. The percentage of ARAP1 signal at mitochondria was calculated as "ARAP1-Mito"/"ARAP1". A total of eight cells were observed. The ratios between cells without CDRs and with CDRs were compared (**D**). *$p < 0.05$ (one-tailed unpaired Student *t*-test). **E-F** PP2A was translocated from mitochondria to CDRs upon EGF stimulation. PP2A was localized to mitochondria prior to EGF stimulation (**E**). PP2A was observed at EGF-stimulated CDRs (**F**). **G-H** RIN1 was used as a negative control for the ARAP1 and PP2A staining experiments. RIN1 was observed at mitochondria prior to EGF stimulation (**G**), but not observed at the EGF-stimulated CDRs (**H**). **I-J** CCCP, a drug that blocks mitochondrial functions, inhibited EGF-induced CDRs in Hep3B cells (**I**) but not in MPC5 cells (**J**). In total, more than 1000 Hep3B cells and 1200 MPC5 cells were counted per experiment to calculate the average number of CDRs per cell. Three independent experiments were performed for the quantification. ***$p < 0.001$ (two-tailed paired Student *t*-test)

area". Compared with the control cells, confocal microscopy revealed an expanded distribution area of TOM20 expression in KO cells (Fig. 5A). Furthermore, the quantification analysis clearly showed that the ratio was slightly, albeit significantly, increased in the KO cells (Fig. 5B), whereas the sizes of cells remained unaltered (Fig. 5C). Therefore, these observations indicated that the mitochondrial distribution area was increased in KO cells. By way of confirmation, we also used the mitochondrial marker TIM23, and accordingly detected an increase in the "area of TIM23"/"cell area" ratio in the KO cells (Supplementary Fig. 6A-C). Although imaging analysis revealed that the distribution area of mitochondria identified by the marker proteins was altered by the depletion of ARAP1, the underlying molecular mechanism was unknown. Mitochondria continuously change structure by undergoing a merging process called mitochondrial fusion and a dividing process called mitochondrial fission [2]. The mitochondrial fission protein 1 (FIS1) is one of the key molecules that regulates mitochondria fission. It has been shown that the expression level of FIS1 is increases during fission, making FIS1 a suitable mitochondria fission marker [3, 19]. Surprisingly, we found that the expression level of FIS1 increased in KO cells compared to that in control cells (Fig. 5D), suggesting that mitochondrial fission was induced by

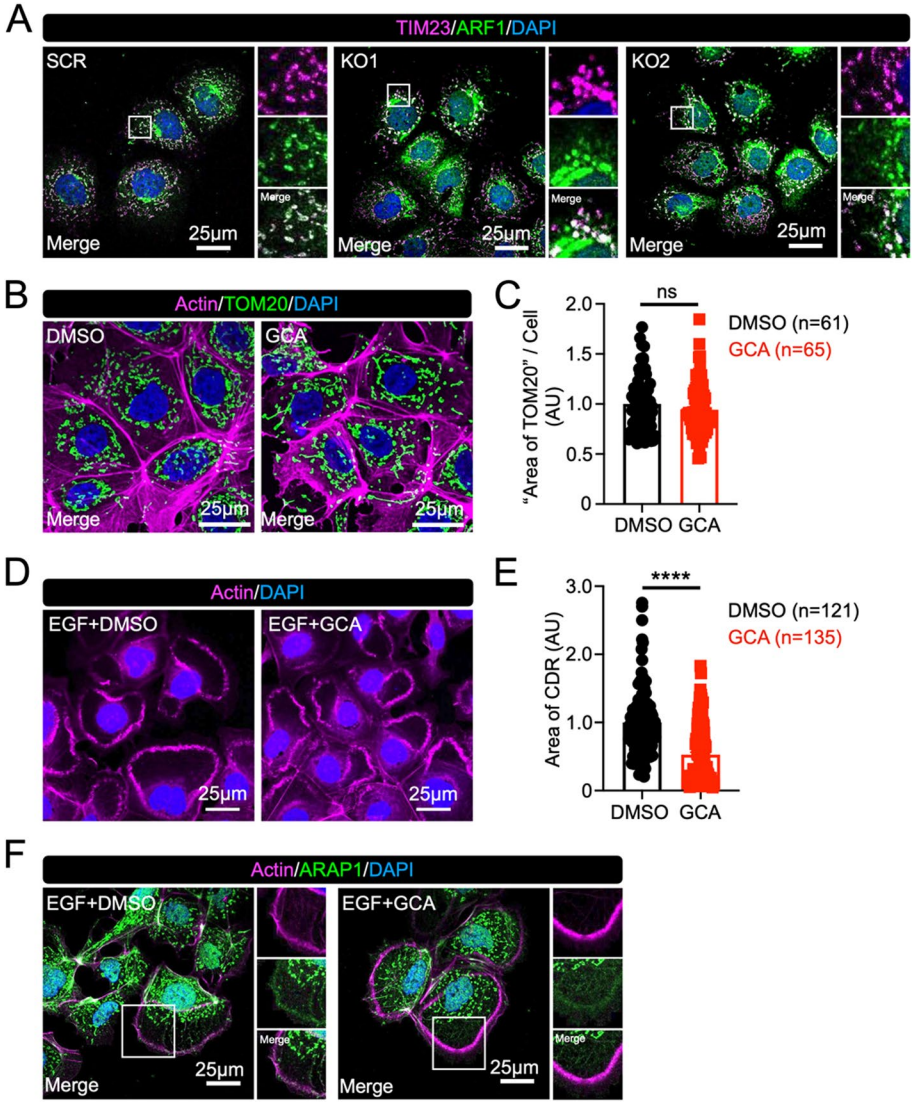

Fig. 7 ARF1 regulates CDR size independently of ARAP1 function. **A** Representative confocal images showing the co-localization of TIM23 (magenta) and ARF1 (green) in both control (SCR) and ARAP1 knockout (KO1 and KO2) cells. **B** and **C** ARF1 inhibitor Golgicide A (GCA) treatment had no appreciable effects on the distribution pattern of TOM20. Representative confocal images of Actin (magenta) and TOM20 (green) without (DMSO)/with (GCA) the ARF1 inhibitor (**B**). Statistical analysis showing that the area of TOM20 distribution remained unchanged after GCA treatment (**C**). $n = 61$ (DMSO) and 65 (GCA), from two-independent experiments. ns: not significant (two-tailed unpaired Student's *t*-test). AU: arbitrary unit. **D** and **E** GCA treatment resulted in a reduction of CDR size.Representative confocal images of EGF-induced CDRs identified by actin (magenta) without (DMSO)/with (GCA) the inhibitor (**D**). Statistical analysis revealed a reduction in CDR area in response to inhibitor treatment (**E**). $n = 121$ (DMSO) and 135 (GCA), from two-independent experiments. ****$p < 0.0001$ (two-tailed unpaired Student's *t*-test). AU: arbitrary unit. **F** Representative confocal images showingthat ARAP1 was localized in EGF-induced CDRs without (DMSO)/with (GCA) the inhibitor

ARAP1 depletion. Because this result was unpredicted, to exclude the possibility of the side effect of KO process of ARAP1, we generated the 3rd KO cell line (KO3) and confirmed that FIS1 expression was increased in the KO cells (Supplementary Fig. 6D and E). Collectively, these findings suggested that ARAP1 is uniquely located at the mitochondria of Hep3B cells and is associated with the molecular mechanisms underlying mitochondrial fission.

Interaction between mitochondrial function and CDR formation in Hep3B cells

Given our finding of the ARAP1 localization at mitochondria, we predicted that mitochondria might be recruited to the CDRs. Contrary to expectations, however, we observed that the distribution patterns of both TIM23 and TOM20 remained virtually unaltered in response to EGF stimulation, and we detected an absence

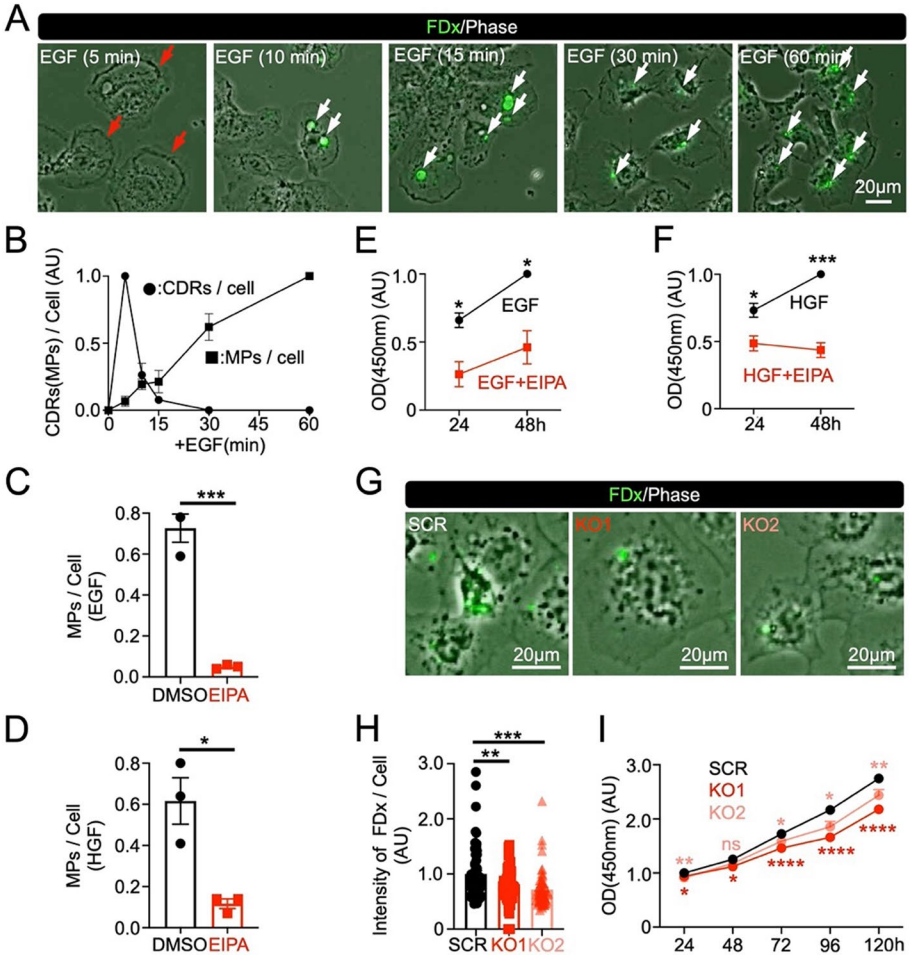

Fig. 8 The CDR–macropinocytosis process functions as a system for the uptake of extracellular nutrients. **A** Image analysis revealed CDRs (red arrows) and macropinosomes (MPs), identified using fluorescein isothiocyanate-labeled dextran with an average molecular weight of 70,000 (FDx70, green) (white arrows), in Hep3B cells following EGF stimulation. **B** Quantitative analysis based on three independent experiments revealed that CDRs were generated within 30 mins after EGF stimulation, with peak production occurring at 5 mins and subsequent development of macropinosomes. **C** and **D** 5-(*N*-Ethyl-*N*-isopropyl)-amiloride (EIPA) treatment inhibited the induction of MPs by EGF (**C**) and HGF (**D**). $n = 3$. ***$p <$ 0.001; *$p < 0.05$ (two-tailed paired Student's *t*-test). **E** and **F** Results of cell counting kit-8 (CCK-8) cell proliferation assays. EIPA treatment attenuated growth factor-induced cell growth in cell culture media containing serum. $n = 3$. ***$p < 0.001$; *$p < 0.05$ (two-tailed paired Student's *t*-test). AU: arbitrary unit. **G** and **H** ARAP1 KO cells were characterized by lower levels of nutrient uptake. Image analysis shows fewer FDx70 signals in the KOs (KO1 and KO2) cells compared with the control (SCR) cells (**G**). Quantitative analysis showing that the total intensity of FDx70 signals in the KO cells was lower than that in the control cells (**H**). Cells were stimulated by EGF for 30 minutes with FDx70, and fixed. The FDx70 signals were measured for each cell and the values were divided by the cell area (intensity of FDx70/cell). $n = 64$ (SCR), 47 (KO1), and 58 (KO2), from two independent experiments. ****$p < 0.0001$ (one-way ANOVA). AU: arbitrary unit. **I** Results of a CCK-8 assay showing that the rates of KO (KO1 and KO2) cell growth were slower than that of the control (SCR) cells in cell culture media containing serum. $n = 3$. ****$p < 0.0001$; **$p < 0.01$; *$p < 0.05$. ns: not significant (one-way ANOVA). AU: arbitrary unit

of signals within the CDRs (Fig. 6A and B). These observations would thus suggest that following GF stimulation, ARAP1 undergoes translocation from the mitochondria to the CDRs. To test this hypothesis, we measured the efficiency of ARAP1 and TIM23 colocalization in cells with or without CDRs (Fig. 6C and D). Using image analysis software, pseudo-images showing ARAP1 at the mitochondria were generated based on the ARAP1 and TIM23 images (Fig. 6C, ARAP1-Mito). Then, the percentage of ARAP1 at mitochondria was calculated as "ARAP1-Mito"/"ARAP1", and the results were compared between cells without CDRs and cells with CDRs (Fig. 6D). Quantitative analysis showed that the ARAP1 signal at mitochondria was decreased in cells with CDRs, suggesting that ARAP1 located at the mitochondria was translocated to CDRs. To identify other proteins transferred from the mitochondria to the CDRs, we screened several proteins involved in mitochondrial functions and/

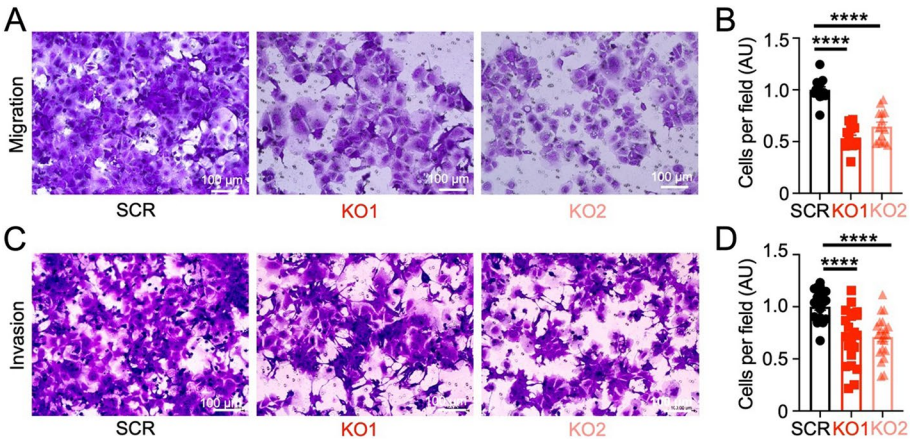

Fig. 9 The involvement of ARAP1 in Hep3B cell malignancy. Transwell migration (**A** and **B**) and invasion (**C** and **D**) assays in vitro showing that the deletion of ARAP1 influenced the malignant potentials of Hep3B cells. More than 10 images from two independent experiments were observed for the assays. Representative images are shown (**A** and **C**). The quantification results are shown as arbitrary unit (AU) (**B** and **D**). ****$p < 0.0001$ (one-way ANOVA)

or observed in the CDRs. Protein phosphatase 2 (PP2A) regulates mitochondria-lysosome crosstalk [7] and mitochondria-associated membrane (MAM) formation [6]. We found that PP2A was localized to the mitochondria without EGF stimulation in Hep3B cells, and the protein was also detected at the CDRs (Fig. 6E and F). In a previous study, we showed that RIN1 protein was not detected at CDRs and used it as a negative control for IF experiments [46]. Interestingly, we found that RIN1 was present at the mitochondria, but not at the CDRs (Fig. 6G and H). Thus, RIN1 can also be used as a negative control for proteins transferred from the mitochondria to CDRs. Finally, to test whether there is a direct interaction between CDR formation and mitochondrial function, we used carbonyl cyanide m-chlorophenyl hydrazone (CCCP), an inhibitor of mitochondrial oxidative phosphorylation that has been used as a drug to block mitochondrial functions [28, 56]. The results showed that CCCP treatment completely blocked EGF-induced CDRs in Hep3B cells (Fig. 6I), but not in MPC5 cells (Fig. 6J). Thus, these results suggest that there is an interaction between mitochondrial function and CDR formation in Hep3B cells and that both ARAP1 and PP2A are involved in this mechanism.

Intracellular protein trafficking mechanism is dysfunctional in Hep3B cells

Our results raised the possibility that aberrant membrane tethering between the mitochondrial surface and the Golgi Apparatus may have occurred in Hep3B cells. Thus, we next sought to observe if there is a difference in the distribution patterns of cargo proteins such as Golgin-97, which is involved in Golgi trafficking mechanisms [44], in Huh7 and Hep3B cells (Supplementary Fig. 7). Confocal microscopy showed that while Golgin-97 was expressed with the expected pattern of Golgi Apparatus structure in Huh7 cells, but the distribution pattern was disturbed in Hep3B cells. Co-localization of Golgin-97 and TIM23 was evident in Huh7 cells. Meanwhile, in Hep3B cells, Golgin-97 signal was observed close to TIM23 signal, but they were not co-localized. This suggested that intracellular protein trafficking mechanisms may be dysfunctional in Hep3B cells. Indeed, when Brefeldin A (BFA) was used to block intracellular trafficking, the distribution patterns of TIM23 in Huh7 cells were altered (Supplementary Fig. 8A) but not in Hep3B cells (Supplementary Fig. 8B). Lastly, we tested whether BFA treatment affected HGF-induced CDRs and found that CDRs were still induced after treatment (Supplementary Fig. 8C). These results suggested that dysfunction of intracellular protein trafficking mechanisms affected the distribution pattern of mitochondria in Hep3B cells.

ARF1 is mitochondrially localized and inhibition of ARF1 function disrupts CDR formation

We also observed that ARF1 was co-localized with TIM23, and confirmed this co-localization in the KO cells (Fig. 7A). To establish whether ARF1 is involved in the mechanisms associated with mitochondrial distribution pattern, we used the ARF1 inhibitor Golgicide A (GCA) [42]. We found that treatment with this inhibitor had no appreciable effects on the distribution pattern of TOM20 (Fig. 7B and C) or on the co-localization of ARF1 and TIM23 (Supplementary Fig. 9A). We also detected the co-localization of ARF1 and TIM23 in Huh7 cells, which would indicate that ARF1 may play a role in mitochondrial localization or function (Supplementary

Fig. 9B). Interestingly, we observed a reduction in the size of CDRs following inhibitor treatment (Fig. 7D and E), and also noted the maintained CDR localization of ARAP1 in inhibitor-treated cells (Fig. 7F).

Depletion of ARAP1 attenuates CDR-mediated macropinocytosis as a nutrient uptake pathway and malignant potential in Hep3B cells

The fluorescent dye FDx70 has previously been used as a representative extracellular solute to measure the efficiency of endocytic ingestion [18, 60], and in the present study, we used this system to determine whether the CDRs in Hep3B cells undergo a transition to macropinosomes. Time-course experiments revealed that whereas CDRs were induced within 5 min following EGF stimulation, they had disappeared when assessed at 15 min, concomitant with an increase in the numbers of vesicles characterized by FDx70 signals, thereby indicating the formation of macropinosomes (Fig. 8A and B). These findings thus indicate that the induction CDRs is a key step in the nutrient uptake pathway of cells. EIPA is known as an established inhibitor of macropinocytosis but not of other endocytosis pathways [47, 55], with demonstrated use in both in vitro [27] and in vivo [10] experiments. We observed that EIPA treatment reduced the number of EGF-mediated induction of macropinosomes (Fig. 8C). We also demonstrated that HGF treatment induced CDRs and macropinosomes (Supplementary Fig. 10), and the formation of these was also inhibited by EIPA treatment (Fig. 8D). Subsequently, to determine whether inhibition of macropinosomes influences GF-stimulated cell growth, we performed cell proliferation assays in the presence or absence of EIPA in cell culture media containing serum with EGF (Fig. 8E) or HGF (Fig. 8F). Compared to the control cells, we detected a reduction in the rate of cell growth in cells exposed to EIPA. These findings suggest that CDR-associated macropinocytosis plays an important role in promoting cell growth, presumably via uptake of extracellular nutrients.

Based on our observations of smaller CDRs in ARAP1 KO cells (Figs. 1D and 2A-B), we speculated that the nutrient uptake mechanism in these cells would be attenuated. Therefore, we next measured the amount of ingested extracellular solutes by comparing the intensities of integrated FDx70 detected in control and KO cells. Cells were stimulated with EGF and incubated with FDx70 for 30 min, as described previously (Fig. 8A). The results revealed a diminished intensity of FDx70 in the KO cells, implying a disruption of the nutrient uptake mechanisms in the KO cells (Fig. 8G and H). Moreover, a cell proliferation assay using control and KO cells in cell culture media containing serum without GF stimulation showed that the rate of KO cell growth was slower than that of control cells (Fig. 8I). Therefore, ARAP1 plays an important role in cell growth.

Finally, given that Hep3B is an HCC cell line, we sought to assess whether the depletion of ARAP1 would influence cell malignancy. For this purpose, we performed Transwell migration and invasion assays to measure cancer cell motility and invasiveness [23, 24, 38, 54]. Cells were cultured on the Transwell insert for 48 h, and the migrated cells were observed at the basal side of the porous membranes (Fig. 9A and B). For the invasion assay, the extracellular matrix was coated on the surface of the insert, and the cells at the basal side of the membranes were observed as invaded cells (Fig. 9C and D). The results clearly revealed that both the migration and invasion capacities of these cells were reduced following ARAP1 KO.

Discussion

In the present study, we investigated the molecular mechanisms and roles of CDRs in Hep3B cells, focusing on the cellular functions of ARAP1. We found that the CDRs in ARAP1 KO cells were smaller in size than those in control cells (Fig. 1D and E, and Fig. 2A and B). Moreover, we established that the deletion of this protein attenuated the efficiency of extracellular solute uptake (Fig. 8G and H), rate of cell growth (Fig. 8I), and migration/invasion behavior (Fig. 9) of cells. These findings provide evidence that by modulating the nutrient uptake pathway mediated via CDR-associated micropinocytosis, ARAP1 may play an important role in the malignant activity of Hep3B cells (Fig. 10). We also observed that ARAP1 was specifically localized to the mitochondria in Hep3B cells (Fig. 3A and B). Interestingly, inhibition of mitochondrial function blocked EGF-induced CDRs in Hep3B cells, but not in MPC5 cells (Fig. 6I and J). Thus, we speculated that the mitochondrial localization of ARAP1 is associated with the induction of CDR formation in Hep3B cells (Fig. 10).

We found that both ARF1 and ARAP1 were at mitochondria in Hep3B cells (Fig. 3A and B, and Fig. 7A). ARF1 was located at mitochondria in the ARAP1 KO cells and with ARF1 inhibitor treatment (Fig. 7A and Supplementary Fig. 9A). Moreover, we established that whereas the deletion of ARAP1 altered the mitochondrial distribution pattern, the inhibition of ARF1 did not (Fig. 5A-C, and Fig. 7B and C). FIS1 expression was increased in the ARAP1 KO cells (Fig. 5D and Supplementary Fig. 6D). Comparison of Golgin-97 and TIM23 observations between Huh7 and Hep3B cells suggested that dysfunction of intracellular trafficking triggers an abnormal distribution pattern of mitochondria in Hep3B cells (Supplementary Figs. 7 and 8). Based on these

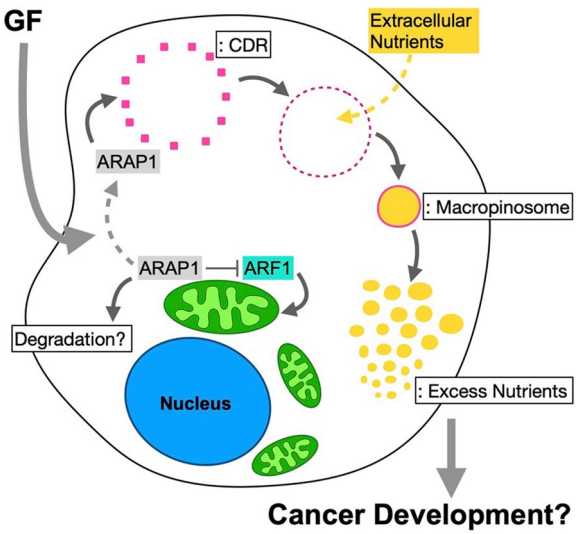

Fig. 10 A proposed model of ARAP1 function and the physiological role of CDRs in Hep3B cells. ARAP1 is specificallylocated at the mitochondria, thereby downregulating the activity of ARF1, which would modulate the mitochondrial distribution pattern. Growth factor stimulation triggers the translocation of ARAP1 from the mitochondria to the CDRs. CDRs comprise small vertical lamellipodia, the distribution of which is regulated by ARAP1. CDRs develop into macropinosomes, resulting in an excessive uptake of nutrients and thus leading to cancer development. Protein degradation mechanisms targeting ARAP1 might be activated

findings, we concluded that mitochondrial fission was hindered by ARAP1 and the distribution pattern of mitochondria was disturbed in Hep3B cells. If so, it could be proposed that the mitochondrial localization of ARAP1 suppresses the activity of ARF1 function, thereby modulating the pattern of mitochondrial distribution in Hep3B cells. Interestingly in this regard, several studies have reported that ARF1 modulates mitochondrial morphology. For example, in *Caenorhabditis elegans*, activation of ARF1 by the guanine nucleotide exchange factor (GEF) GFB1 has been established to regulate the interactions between the endoplasmic reticulum (ER) and mitochondria, which results in the formation of a complex referred to as the ER–mitochondria encounter structure (ERMES) [1, 45], and in *Candida albicans*, the deletion of ARF1 has been found to induce the formation of ERMES [62]. The role of the GBF1–ARF1 pathway in mitochondria has also been examined in human retinal pigment epithelial RPE1 cells [53], whereas in HeLa cells, deletion of GBF1 has been demonstrated to induce the condensation of mitochondrial networks. In the present study, our finding that ARF1, although not ARAP1, is localized at the mitochondria of Huh7 cells (Supplementary Fig. 9B), indicates that the activation of mitochondrially localized ARF1 may play an important role in determining the cellular distribution of these organelles. Consequently, we hypothesize that by suppressing ARF1 activity, ARAP1 at the mitochondria would disrupt the mitochondrial distribution pattern in Hep3B cells (Fig. 10).

On the basis of confocal microscopy observations, we established that ARAP1 is also located at the CDRs of Hep3B cells, which could provide evidence that in response to GF stimulation, ARAP1 is translocated from the mitochondria to the CDRs, although at present the underlying molecular mechanisms remain unclear. Interestingly in this context, it has previously been shown that mitochondrial overexpression of the ARF1-GAP ASAP1 has the effect of inhibiting the spread and migration of REF52 rat embryo fibroblasts [32]. In the present study, we found that deletion of ARAP1 resulted in a reduction in the size of CDRs (Fig. 1D and E and 2 A and B) and disruption of the expression patterns of small vertical lamellipodia in ARAP1 KO cells (Fig. 2C and Supplementary Fig. 3B). Thus, it can be reasoned that a downregulation of ARF1 induced by the mitochondrial localization of ARAP1 might have an influence on the cytoskeletal mechanisms associated with the formation of CDRs (Fig. 10). Accordingly, further studies are warranted to elucidate the molecular mechanisms and cellular function of mitochondrially expressed ARAP1 in Hep3B cells.

We also established that inhibition of ARF1 similarly resulted in a reduction in the size of CDRs, (Fig. 7D and E), even though we were unable to detect this protein in the CDRs (Fig. 1B). Given that ARAP1 was found to be localized in the CDRs, even after ARF inhibitor treatment (Fig. 7F), we speculate that ARF1 and ARAP1 contribute independently to the regulation of CDR formation. In previous studies that have examined the roles of ARF1 and other ARFs in CDR formation, Hasegawa et al. observed the localization of GFP-ARF1 in the PDGF-induced CDRs of NIH-3T3 cells [14], and also found that overexpression of the dominant-negative forms of ARF1 and ARF5 induced larger-sized CDRs. Furthermore, it has been demonstrated that ARF6 regulates CDRs as a downstream signaling molecule of NUMB-EFA6B pathway [67]. EFA6B is one of the ARF6 GEFs [11], and these authors revealed that EFA6B is regulated by the tumor suppressor NUMB, the deletion of which (presumably leading to the deactivation of ARF6) was associated with an increase in the number of CDRs induced by HGF in HeLa cells, as well as that induced by PDGF in MEFs. It has also been shown that overexpression of the dominant-active form of ARF6 (Q67L) is associated with a reduction in the numbers of PDGF-induced CDRs in NIH-3T3 cells [14]. In the present study, we similarly observed that both NUMB and ARF6 are CDR localized in Hep3B cells (Supplementary Fig. 1A and B). Although the precise mechanisms have yet to be established, these findings provide evidence that ARFs 1, 5,

and 6 coordinately regulate CDR development via GAPs and GEFs. Further studies using the same cell types and ligand sets should be conducted to elucidate the roles of each of these molecules in CDR formation.

In addition to its unique cellular localization, our data showed that the expression level of ARAP1 in Hep3B cells was lower than that in control cells (Fig. 4A). This suggests that the expression mechanism of ARAP1 is disturbed or that protein degradation mechanisms targeting ARAP1 are continuously activated in Hep3B cells. Indeed, ARAP1 expression level in Hep3B, but not in Huh7, was increased by MG132 treatment (Fig. 4B and C). In addition, we observed that GFP-ARAP1 could be expressed in 293T and Huh7 cells, but not in Hep3B cells (Supplementary Fig. 4A-C). Based on these results, we speculate that ARAP1 is stringently regulated, and possibly by overactive degradation in Hep3B cells (Fig. 10). There are three different protein degradation mechanisms: autophagy, unfolded protein response (UPR) and ER-associated protein degradation (ERAD) [15, 26, 40]. Among them, the UPR and ERAD function in the ER. Since we observed clear mitochondrial localization of ARAP1, the protein may be degraded in the mitochondria, suggesting a process related to mitophagy. Meanwhile, our data suggest that ARAP1 has a cellular function in regulating mitochondrial distribution patterns. If this is the case, mitochondrial localization of ARAP1 would not be involved in the degradation process, but as a part of the cellular function. Meanwhile, confocal microscopy showed that nuclear expression of ARAP1 was apparent in Huh7 cells (Supplementary Fig. 5A) and that ARAP1 expression in nuclei was increased after MG132 treatment in Hep3B cells (Supplementary Fig. 5B). Therefore, it could be proposed that ARAP1 in the cytosol is the predominant target of protein degradation mechanisms. This hypothesis reflects one of the future research directions to identify further details of the molecular mechanisms of ARAP1 expression in Hep3B cells.

Transwell migration and invasion assays showed that the depletion of ARAP1 affected the malignant potential of Hep3B cells (Fig. 9). Since macropinocytosis regulates the AKT and mTORC1 pathways [48], which are involved in tumor cell motility and invasion [9, 66], it could be predicted that the dysfunction of CDRs in ARAP1 KO cells would disturb these pathways, resulting in reduced migration and invasion ability. Meanwhile, we observed that the ARAP1 expression level in Hep3B cells was lower than that in the control cells that do not present CDRs (Fig. 4A). Given that our data suggested that ARAP1 downregulates mitochondrial fission, we also hypothesize that expression level of ARAP1 would affect the function of mitochondria in Hep3B cells. To elucidate the role of ARAP1 in cancer development, further studies should focus on at least three aspects: the molecular mechanisms of ARAP1 degradation, the role of ARAP1 in mitochondrial fission, and the function of ARAP1 in CDRs.

Conclusions

In this study, we characterized the roles of ARAP1 with respect to the development of circular dorsal ruffles (CDRs) in Hep3B cells. Our findings indicate that ARAP1 regulates both CDR formation and the pattern of mitochondrial distribution, which leads us to speculate on a mechanistic interaction between CDR formation and mitochondrial function in Hep3B cells. Scanning electron micrographs revealed that CDRs comprise small-sized vertical lamellipodia, the expression pattern of which was observed to be disrupted in response to the deletion of ARAP1. Accordingly, it is conceivable that as an initial step in the induction of CDR, the cellular locations of the mitochondria might determine the distribution of individual lamellipodia. As to the cellular function of these structures, our data clearly reveal that CDRs could play an important role in the nutrient uptake of Hep3B cells in response to growth factor stimulation. Given that CDRs are not exposed on the surfaces of other types of HCC cells, such as HepG2 and Huh7, or the LO2 cell line [46], it can be predicted that nutrients taken up via CDRs might abnormally influence the anabolic and catabolic processes of Hep3B cells. If this is indeed the case, as CDRs have been observed in certain other types of cancer cells, it is reasonable to assume that the excess uptake of nutrients is associated with cancer development. Our finding that ARAP1 was specifically localized at mitochondria in Hep3B cells, and the protein expression level was lower than in control cells, suggested that aberrant expression of ARAP1 affects the CDR formation. Given the important implications of these findings, we believe that the molecular mechanisms underlying the formation of CDRs focusing on ARAP1 could serve as an effective therapeutic target in some types of cancer.

Abbreviations

ARAP1	Arf-GAP with Rho-GAP domain, Ankyrin repeat and PH domain 1
AU	Arbitrary unit
BFA	Brefeldin A
BSA	Bovine serum albumin
CCCP	Carbonyl cyanide m-chlorophenyl hydrazone
CDR	Circular dorsal ruffle
EGF	Epidermal growth factor
EIPA	5-(*N*-Ethyl-*N*-isopropyl)-amiloride
FDx70	Fluorescein isothiocyanate-labeled dextran with an average molecular weight of 70,000
GCA	Golgicide A
GFP	Green fluorescent protein
HCC	Hepatocellular Carcinoma
HGF	Hepatocyte growth factor
IF	Immunofluorescence
KO	Knockout
MP	Macropinosome

PFA	Paraformaldehyde
PP2A	Protein phosphatase 2
RT	Room temperature
SCR	Scramble
SEM	Scanning electron microscopy

Supplementary Information

The online version contains supplementary material available at https://doi.org/10.1186/s12964-025-02084-4.

Supplementary Infomation

Supplementary Material 1.

Acknowledgements
This study was supported by the Frontiers Science Center for Cell Responses Grant from Nankai University (C029205001) (SY), the Tianjin Key Medical Discipline (Specialty) Construction Project (SY), Shenzhen Science and Technology Program (Grant No. JCYJ20210324120813037) (SY), National Science Foundation of China (82250610231) (ACM), the Key Discipline Special Project of Tianjin Municipal Health Commission (TJWJ2022XK016) (WJ), and the Key Project of Tianjin Science and Technology Bureau Applied Basic Research (23JCZDJC01200) (WJ). XS was supported by the Tianjin Graduate Students Scientific Research Innovation Project (2021YJSB087).

Authors' contributions
XS and YL designed and performed the experiments, with the support from YH, LC, JW, Jc, and LD. SY conceived the study, designed the experiments, and wrote the manuscript, with the support from ZS, YX, ACM, and WJ.

Data availability
No datasets were generated or analysed during the current study.

Declarations

Competing interests
The authors declare no competing interests.

Author details
[1]State Key Laboratory of Medicinal Chemical Biology, College of Life Sciences, Frontiers Science Center for Cell Responses, Nankai University, Tianjin, China. [2]Organ Transplant Department, School of Medicine, Tianjin First Central Hospital, Nankai University, Tianjin, China. [3]Research Institute of Transplant Medicine, Nankai University, Tianjin, China. [4]Tianjin Key Laboratory for Organ Transplantation, Tianjin, China. [5]Tianjin Key Laboratory of Molecular Diagnosis and Treatment of Liver Cancer, Tianjin First Center Hospital, Tianjin 300384, China. [6]Liver Transplantation Department, Tianjin First Center Hospital, Tianjin, China. [7]Key Laboratory of Bioactive Materials, Ministry of Education, College of Life Sciences, Nankai University, Tianjin 300071, China. [8]Nankai International Advanced Research Institute, Shenzhen, China. [9]Nankai University College of Life Sciences, Tianjin, 300071, China.

Received: 25 October 2024 Accepted: 5 February 2025
Published online: 11 February 2025

References

1. Ackema KB, Hench J, Bockler S, Wang SC, Sauder U, Mergentaler H, Westermann B, Bard F, Frank S, Spang A. The small GTPase Arf1 modulates mitochondrial morphology and function. EMBO J. 2014;33:2659–75.
2. Adebayo M, Singh S, Singh AP, Dasgupta S. Mitochondrial fusion and fission: the fine-tune balance for cellular homeostasis. FASEB J. 2021;35:e21620.
3. Aksu-Menges E, Eylem CC, Nemutlu E, Gizer M, Korkusuz P, Topaloglu H, Talim B, Balci-Hayta B. Reduced mitochondrial fission and impaired energy metabolism in human primary skeletal muscle cells of Megaconial congenital muscular dystrophy. Sci Rep. 2021;11:18161.
4. Bagnato P, Castagnino A, Cortese K, Bono M, Grasso S, Bellese G, Daniele T, Lundmark R, Defilippi P, Castagnola P, et al. Cooperative but distinct early co-signaling events originate from ERBB2 and ERBB1 receptors upon trastuzumab treatment in breast cancer cells. Oncotarget. 2017;8:60109–22.
5. Boscher C, Nabi IR. Galectin-3- and phospho-caveolin-1-dependent outside-in integrin signaling mediates the EGF motogenic response in mammary cancer cells. Mol Biol Cell. 2013;24:2134–45.
6. Chaiwijit P, Uppakara K, Asavapanumas N, Saengsawang W. The effects of PP2A disruption on ER-mitochondria contact and mitochondrial functions in neuronal-like cells. Biomedicines. 2023;11:1011.
7. Che L, Wu JS, Xu CY, Cai YX, Lin JX, Du ZB, Shi JZ, Han T, He YQ, Lin YC, et al. Protein phosphatase 2A-B56gamma-Drp1-Rab7 signaling axis regulates mitochondria-lysosome crosstalk to sensitize the anti-cancer therapy of hepatocellular carcinoma. Biochem Pharmacol. 2022;202:115132.
8. Chen PW, Jian X, Heissler SM, Le K, Luo R, Jenkins LM, Nagy A, Moss J, Sellers JR, Randazzo PA. The Arf GTPase-activating protein, ASAP1, binds nonmuscle myosin 2A to control remodeling of the actomyosin network. J Biol Chem. 2016;291:7517–26.
9. Chin YR, Toker A. Function of Akt/PKB signaling to cell motility, invasion and the tumor stroma in cancer. Cell Signal. 2009;21:470–6.
10. Commisso C, Davidson SM, Soydaner-Azeloglu RG, Parker SJ, Kamphorst JJ, Hackett S, Grabocka E, Nofal M, Drebin JA, Thompson CB, et al. Macropinocytosis of protein is an amino acid supply route in Ras-transformed cells. Nature. 2013;497:633–7.
11. Derrien V, Couillault C, Franco M, Martineau S, Montcourrier P, Houlgatte R, Chavrier P. A conserved C-terminal domain of EFA6-family ARF6-guanine nucleotide exchange factors induces lengthening of microvilli-like membrane protrusions. J Cell Sci. 2002;115:2867–79.
12. Gu Z, Noss EH, Hsu VW, Brenner MB. Integrins traffic rapidly via circular dorsal ruffles and macropinocytosis during stimulated cell migration. J Cell Biol. 2011;193:61–70.
13. Ha VL, Bharti S, Inoue H, Vass WC, Campa F, Nie Z, de Gramont A, Ward Y, Randazzo PA. ASAP3 is a focal adhesion-associated Arf GAP that functions in cell migration and invasion. J Biol Chem. 2008;283:14915–26.
14. Hasegawa J, Tsujita K, Takenawa T, Itoh T. ARAP1 regulates the ring size of circular dorsal ruffles through Arf1 and Arf5. Mol Biol Cell. 2012;23:2481–9.
15. Hetz C, Zhang K, Kaufman RJ. Mechanisms, regulation and functions of the unfolded protein response. Nat Rev Mol Cell Biol. 2020;21:421–38.
16. Hoon JL, Wong WK, Koh CG. Functions and regulation of circular dorsal ruffles. Mol Cell Biol. 2012;32:4246–57.
17. Hooshmand-Rad R, Claesson-Welsh L, Wennstrom S, Yokote K, Siegbahn A, Heldin CH. Involvement of phosphatidylinositide 3'-kinase and Rac in platelet-derived growth factor-induced actin reorganization and chemotaxis. Exp Cell Res. 1997;234:434–41.
18. Hua R, Wei J, Torres M, He Y, Li Y, Sun X, Wang L, Inoki K, Yoshida S. Identification of circular dorsal ruffles as signal platforms for the AKT pathway in glomerular podocytes. J Cell Physiol. 2023;238:1063–79.
19. Ihenacho UK, Meacham KA, Harwig MC, Widlansky ME, Hill RB. Mitochondrial fission protein 1: emerging roles in organellar form and function in health and disease. Front Endocrinol (Lausanne). 2021;12:660095.
20. Itoh T, Hasegawa J. Mechanistic insights into the regulation of circular dorsal ruffle formation. J Biochem. 2013;153:21–9.
21. Jackson TR, Brown FD, Nie Z, Miura K, Foroni L, Sun J, Hsu VW, Donaldson JG, Randazzo PA. ACAPs are arf6 GTPase-activating proteins that function in the cell periphery. J Cell Biol. 2000;151:627–38.
22. Jiang YH, Zhu XY, Guo ZY, Yang ZH. Increased long non-coding RNA ARAP1-AS1 expression and its prognostic significance in human gastric cancer: a preliminary study. Eur Rev Med Pharmacol Sci. 2020;24:1815–20.
23. Justus CR, Leffler N, Ruiz-Echevarria M, Yang LV. In vitro cell migration and invasion assays. J Vis Exp. 2014.
24. Justus CR, Marie MA, Sanderlin EJ, Yang LV. Transwell in vitro cell migration and invasion assays. Methods Mol Biol. 2023;2644:349–59.
25. Kadrmas JL, Beckerle MC, Yoshigi M. Genetic analyses in mouse fibroblast and melanoma cells demonstrate novel roles for PDGF-AB ligand and PDGF receptor alpha. Sci Rep. 2020;10:19303.
26. Kawabata T, Yoshimori T. Autophagosome biogenesis and human health. Cell Discov. 2020;6:33.

27. Koivusalo M, Welch C, Hayashi H, Scott CC, Kim M, Alexander T, Touret N, Hahn KM, Grinstein S. Amiloride inhibits macropinocytosis by lowering submembranous pH and preventing Rac1 and Cdc42 signaling. J Cell Biol. 2010;188:547–63.
28. Koncha RR, Ramachandran G, Sepuri NBV, Ramaiah KVA. CCCP-induced mitochondrial dysfunction - characterization and analysis of integrated stress response to cellular signaling and homeostasis. FEBS J. 2021;288:5737–54.
29. Lanzetti L, Palamidessi A, Areces L, Scita G, Di Fiore PP. Rab5 is a signalling GTPase involved in actin remodelling by receptor tyrosine kinases. Nature. 2004;429:309–14.
30. Li C, Dong B, Xu X, Li Y, Wang Y, Li X. Correction to: LncRNA ARAP1-AS1 aggravates the malignant phenotypes of ovarian cancer cells through sponging mir-4735-3p to enhance PLAGL2 expression. Cytotechnology. 2022;74:201.
31. Li F, Miao L, Xue T, Qin H, Mondal S, Thompson PR, Coonrod SA, Liu X, Zhang X. Inhibiting PAD2 enhances the anti-tumor effect of docetaxel in tamoxifen-resistant breast cancer cells. J Exp Clin Cancer Res. 2019;38:414.
32. Liu Y, Yerushalmi GM, Grigera PR, Parsons JT. Mislocalization or reduced expression of Arf GTPase-activating protein ASAP1 inhibits cell spreading and migration by influencing Arf1 GTPase cycling. J Biol Chem. 2005;280:8884–92.
33. Lu C, Wang X, Zhao X, Xin Y, Liu C. Long non-coding RNA ARAP1-AS1 accelerates cell proliferation and migration in breast cancer through miR-2110/HDAC2/PLIN1 axis. Biosci Rep. 2020;40:BSR20191764.
34. Mellstroom K, Hoglund AS, Nister M, Heldin CH, Westermark B, Lindberg U. The effect of platelet-derived growth factor on morphology and motility of human glial cells. J Muscle Res Cell Motil. 1983;4:589–609.
35. Nie Z, Stanley KT, Stauffer S, Jacques KM, Hirsch DS, Takei J, Randazzo PA. AGAP1, an endosome-associated, phosphoinositide-dependent ADP-ribosylation factor GTPase-activating protein that affects actin cytoskeleton. J Biol Chem. 2002;277:48965–75.
36. Orth JD, Krueger EW, Weller SG, McNiven MA. A novel endocytic mechanism of epidermal growth factor receptor sequestration and internalization. Cancer Res. 2006;66:3603–10.
37. Palamidessi A, Frittoli E, Garre M, Faretta M, Mione M, Testa I, Diaspro A, Lanzetti L, Scita G, Di Fiore PP. Endocytic trafficking of Rac is required for the spatial restriction of signaling in cell migration. Cell. 2008;134:135–47.
38. Pijuan J, Barcelo C, Moreno DF, Maiques O, Siso P, Marti RM, Macia A, Panosa A. In vitro cell Migration, Invasion, and adhesion assays: from cell imaging to data analysis. Front Cell Dev Biol. 2019;7: 107.
39. Puccini J, Badgley MA, Bar-Sagi D. Exploiting cancer's drinking problem: regulation and therapeutic potential of macropinocytosis. Trends Cancer. 2022;8:54–64.
40. Qi L, Tsai B, Arvan P. New insights into the physiological role of endoplasmic reticulum-associated degradation. Trends Cell Biol. 2017;27:430–40.
41. Qiu Z, Liu W, Zhu Q, Ke K, Zhu Q, Jin W, Yu S, Yang Z, Li L, Sun X, et al. The role and therapeutic potential of macropinocytosis in cancer. Front Pharmacol. 2022;13: 919819.
42. Saenz JB, Sun WJ, Chang JW, Li J, Bursulaya B, Gray NS, Haslam DB. Golgicide A reveals essential roles for GBF1 in Golgi assembly and function. Nat Chem Biol. 2009;5:157–65.
43. Sayyed UMH, Mahalakshmi R. Mitochondrial protein translocation machinery: from TOM structural biogenesis to functional regulation. J Biol Chem. 2022;298: 101870.
44. Shin JJH, Gillingham AK, Begum F, Chadwick J, Munro S. TBC1D23 is a bridging factor for endosomal vesicle capture by golgins at the trans-golgi. Nat Cell Biol. 2017;19:1424–32.
45. Spang A. A small GTPase involved in mitochondrial morphology and function. Biochem Soc Trans. 2015;43:108–10.
46. Sun X, Liu Y, Zhou S, Wang L, Wei J, Hua R, Shen Z, Yoshida S. Circular dorsal ruffles disturb the growth factor-induced PI3K-AKT pathway in hepatocellular carcinoma Hep3B cells. Cell Commun Signal. 2022;20:102.
47. Swanson JA, Watts C. Macropinocytosis. Trends Cell Biol. 1995;5:424–8.
48. Swanson JA, Yoshida S. Macropinosomes as units of signal transduction. Philos Trans R Soc Lond B Biol Sci. 2019;374:20180157.
49. Sztul E, Chen PW, Casanova JE, Cherfils J, Dacks JB, Lambright DG, Lee FS, Randazzo PA, Santy LC, Schurmann A, et al. ARF GTPases and their GEFs and GAPs: concepts and challenges. Mol Biol Cell. 2019;30:1249–71.
50. Tanna CE, Goss LB, Ludwig CG, Chen PW. Arf GAPs as regulators of the actin cytoskeleton-an update. Int J Mol Sci. 2019;20:442.
51. Tao X, Zhang Y, Li J, Ni Z, Tao Z, You Q, He Z, Huang D, Zheng S. Low expression of long non-coding RNA ARAP1-AS1 can inhibit lung cancer proliferation by inducing G0/G1 cell cycle organization. J Thorac Dis. 2020;12:7326–36.
52. Teng J, Ai X, Jia Z, Wang K, Guan Y, Guo Y. Long non-coding RNA ARAP1-AS1 promotes the progression of bladder cancer by regulating miR-4735-3p/NOTCH2 axis. Cancer Biol Ther. 2019;20:552–61.
53. Walch L, Pellier E, Leng W, Lakisic G, Gautreau A, Contremoulins V, Verbavatz JM, Jackson CL. GBF1 and Arf1 interact with Miro and regulate mitochondrial positioning within cells. Sci Rep. 2018;8:17121.
54. Wang F, Qiao Y, Yu J, Ren X, Wang J, Ding Y, Zhang X, Ma W, Ding Y, Liang L. FBX8 acts as an invasion and metastasis suppressor and correlates with poor survival in hepatocellular carcinoma. PLoS One. 2013;8:e65495.
55. West MA, Bretscher MS, Watts C. Distinct endocytotic pathways in epidermal growth factor-stimulated human carcinoma A431 cells. J Cell Biol. 1989;109:2731–9.
56. Yan C, Gong L, Chen L, Xu M, Abou-Hamdan H, Tang M, Desaubry L, Song Z. PHB2 (prohibitin 2) promotes PINK1-PRKN/Parkin-dependent mitophagy by the PARL-PGAM5-PINK1 axis. Autophagy. 2020;16:419–34.
57. Yang Y, Lv X, Fan Q, Wang X, Xu L, Lu X, Chen T. Analysis of circulating lncRNA expression profiles in patients with diabetes mellitus and diabetic nephropathy: differential expression profile of circulating lncRNA. Clin Nephrol. 2019;92:25–35.
58. Yoshida S, Pacitto R, Inoki K, Swanson J. Macropinocytosis, mTORC1 and cellular growth control. Cell Mol Life Sci. 2018;75:1227–39.
59. Yoshida S, Pacitto R, Sesi C, Kotula L, Swanson JA. Dorsal ruffles enhance activation of akt by growth factors. J Cell Sci. 2018;131:jcs220517.
60. Yoshida S, Pacitto R, Yao Y, Inoki K, Swanson JA. Growth factor signaling to mTORC1 by amino acid-laden macropinosomes. J Cell Biol. 2015;211:159–72.
61. Zdzalik-Bielecka D, Poswiata A, Kozik K, Jastrzebski K, Schink KO, Brewinska-Olchowik M, Piwocka K, Stenmark H, Miaczynska M. The GAS6-AXL signaling pathway triggers actin remodeling that drives membrane ruffling, macropinocytosis, and cancer-cell invasion. Proc Natl Acad Sci U S A. 2021;118:e2024596118.
62. Zhang B, Yu Q, Huo D, Li J, Liang C, Li H, Yi X, Xiao C, Zhang D, Li M. Arf1 regulates the ER-mitochondria encounter structure (ERMES) in a reactive oxygen species-dependent manner. FEBS J. 2018;285:2004–18.
63. Zhang W, Zhang J, Hu Z, Sun W, Xu L, Chu H, Wang X, Fu Q. LncRNA ARAP1-AS1 promotes bladder cancer development by regulating the miR-3918/KIF20A Axis. Mol Biotechnol. 2022;64:1259–69.
64. Zhao F, Zou MH. Role of the mitochondrial protein import machinery and protein processing in heart disease. Front Cardiovasc Med. 2021;8: 749756.
65. Zhong L, Zhong X. Long non-coding RNA ARAP1-AS1 contributes to cell proliferation and migration in clear cell renal cell carcinoma via the miR-361-3p/placental growth factor axis. Bioengineered. 2021;12:6629–42.
66. Zhou H, Huang S. Role of mTOR signaling in tumor cell motility, invasion and metastasis. Curr Protein Pept Sci. 2011;12:30–42.
67. Zobel M, Disanza A, Senic-Matuglia F, Franco M, Colaluca IN, Confalonieri S, Bisi S, Barbieri E, Caldieri G, Sigismund S, et al. A NUMB-EFA6B-ARF6 recycling route controls apically restricted cell protrusions and mesenchymal motility. J Cell Biol. 2018;217:3161–82.

Publisher's Note